Pergamon

Bioorganic & Medicinal Chemistry Letters, Vol. 4, No. 20, pp. 2435-2440, 1994

0960-894X/94 $7.00+0.00

0960-894X(94)00354-8

MULTIPLE BINDING MODES WITH DNA OF ANTHRACENE-9-CARBONYL-N^1-SPERMINE PROBED BY LD, CD, NORMAL ABSORPTION, AND MOLECULAR MODELLING COMPARED WITH THOSE OF SPERMIDINE AND SPERMINE

Gareth Adlam, Ian S. Blagbrough*, Steven Taylor, Harriet C. Latham†, Ian S. Haworth¶, and Alison Rodger†*

School of Pharmacy and Pharmacology, University of Bath, Claverton Down, Bath BA2 7AY, U.K. and

†Physical Chemistry Laboratory, University of Oxford, South Parks Road, Oxford OX1 3QZ, U.K. and

¶Department of Pharmaceutical Sciences, University of Southern California, 1985 Zonal Avenue, Los Angeles, CA 90033, U.S.A.

Abstract: DNA groove-binding and intercalative binding modes of anthracene-9-carbonyl-N^1-spermine have been probed using linear and circular dichroism, and normal absorption techniques. Despite its lower positive charge, anthracene-9-carbonyl-N^1-spermine stabilises DNA more than does spermine and significantly more than spermidine. Data interpretation has been facilitated by molecular modelling.

Natural polyamines bind strongly to cellular DNA. The interaction of polycationic species with DNA is being studied as a possible strategy for the selective design of anti-viral and anti-cancer agents [1-4]. In particular natural polyamines such as spermidine (**1**) and spermine (**2**) are essential for cell proliferation [5] and therefore depletion of intracellular spermine (**2**) levels, and replacement by a synthetically modified polyamine analogue, offers a novel approach in this area of drug design [6]. In order to study these ligand-DNA interactions, we are investigating (**1**), (**2**), and, in particular, anthracene-9-carbonyl-N^1-spermine (**3**) as potential ligands. The conjugate (**3**) was designed as a UV active mimic of the otherwise invisible polyamines since there are considerable difficulties in analysing the DNA interactions of (**1**) and (**2**) due to their lack of a spectroscopically detectable chromophore and their short residence time on DNA [7].

Polyamines are essentially fully protonated at physiological pH. Spermine (**2**) and related polyamines induce a variety of structural changes in DNA including aggregation, condensation, the B-to-Z transition, and DNA bending [8, 9]. Our current research into the structure-activity relationships of DNA-polyamine interactions is focused on understanding this behaviour as a function of the distance between the ammonium ions in the polyamine moiety [10-12]. In this *Letter*, we present the results of experiments to characterize spectroscopically calf thymus DNA (ct-DNA) interactions with the polyamines (**1**) and (**2**), and the conjugate (**3**), using normal absorption, linear dichroism (LD), circular dichroism (CD), and computer modelling.

Spermine conjugate (**3**) was prepared by the selective monoacylation of a primary amino functional group in spermine (**2**), in the presence of the unprotected secondary amines, with commercially available anthracene-9-carboxylic acid. In a typical procedure, the acid was activated with dicyclohexylcarbodiimide, in dichloromethane-tetrahydrofuran (8:1), and coupled with the symmetrical polyamine at 25°C over 4 h. The desired product was separated from the unreacted excess of spermine (**2**) (from 1.5 equiv.) by flash chromatography over silica gel (eluant 8:5:1 CH_2Cl_2-MeOH-conc. NH_4OH). Spermine conjugate (**3**) was obtained as a white solid (85 mg, 17%) which was lyophilized prior to spectroscopic evaluation. Satisfactory spectroscopic [^1H and ^{13}C NMR, ir ν_{max} (KBr disc) 1650 cm^{-1}, and uv λ_{max} (H_2O) 253 nm ε = 108,580; λ_{max} (EtOH) 254 nm ε = 108,950], chromatographic (homogeneous, tlc on silica, UV or ninhydrin detection, eluant CH_2Cl_2-MeOH-conc. NH_4OH 8:5:1 v/v/v), and physical data (mp 97-101°C) were obtained for previously unreported (**3**), [CI ms (isobutane) found 407 $(M+H)^+$; $C_{25}H_{34}N_4O$ requires 406].

The normal absorbance spectra of (**3**) in the absence and presence of ct-DNA are shown in Figs. 1 and 2 respectively. The absorbance of the ligand complexed to DNA (Fig. 3) is determined by subtracting the pure DNA spectrum from that of the DNA-ligand complex. The ligand spectra are thus seen to be significantly less structured when the ligand is bound to DNA than when it is free in solution. Further, the binding of (**3**) to ct-DNA is, in someways, an average of its binding to poly(dG-dC).poly(dG-dC) and poly(dA-dT).poly(dA-dT), referred to as GC and AT respectively. For example, the induced CD (ICD) spectra of (**3**) with GC and AT have opposite signs [13], and the ICD with ct-DNA is significantly smaller in magnitude, but resembles that of GC which is larger than AT. The ICD spectra (Fig. 4) have a constant form (although not sufficiently uniform for the intrinsic method to be used to determine the equilibrium binding constant) until the ligand concentration has increased to a DNA phosphate-ligand mixing ratio of 5:1. A gross structural change, corresponding to condensation, occurs at ~2:1 as it does with GC [13]. The -LD spectra of (**3**) in ct-DNA (180 μM) are shown in Fig. 5. The low ligand concentration LD (-LLD)[13] spectra (Fig. 6) mimic the ligand absorbance spectra (Fig. 3), with the ratio of their magnitudes being the same as the pure ct-DNA LD and absorbance. This, together with the smoothing out of the structure in the absorption spectra, indicates that the anthracene moiety of (**3**) binds intercalatively with ct-DNA. At higher ligand concentrations (Fig. 7), a binding mode that has a negative -LLD signal is evident. As a negative -LLD requires the long axis of the anthracene/helix axis angle to be less then 54.7°, the anthracene cannot be intercalated. As this mode has both ICD and LLD spectra, we conclude that this second mode has a well-defined geometry with the anthracene groove-bound. The decreased orientation of DNA with increased ligand concentration, as shown by LD, indicates conjugate (**3**) bends DNA in the second binding mode. Spermidine (**1**) and spermine (**2**) exhibit similar behaviour.

We also performed DNA melting experiments on ct-DNA with (**1**), (**2**), and (**3**) at mixing ratios of 10:1, in order to probe further the detail of the binding of (**3**) to DNA. As the ligand dominates the absorbance at 260 nm, these experiments were performed at 270 nm (Fig. 8) and also at 280 nm (not shown). The derivatives of the melting curves (not shown) were used to determine the temperature midpoints of the structural transitions including melting. They show that both (**2**) and (**3**) have a premelting transition at ~40°C and 52°C respectively. This is below the melting transition of pure ct-DNA (70°C). As far as we are aware, this small, yet reproducible premelting transition for (**2**) with ct-DNA has not been previously reported.

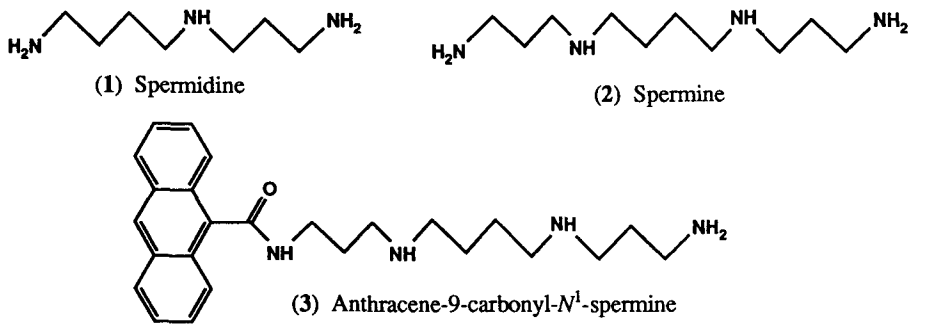

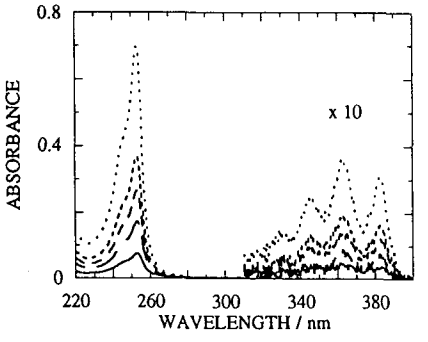

Fig. 1 Normal absorbance spectrum of (3) in 5 mM NaCl, 1 mm pathlength. (3) concentrations: —— 7 μM, — — — 16 μM, – – – 24 μM, ----- 30 μM, ... 53 μM.

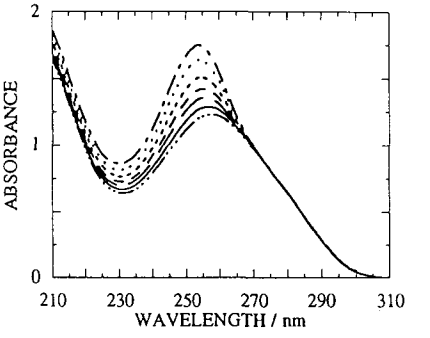

Fig. 2 Normal absorbance spectrum of (3) in 180 μM calf thymus DNA, 5 mM NaCl, 1 mm pathlength. (3) concentrations: —...—... 0 μM, —— 2 μM, — — — 4 μM, – – – 5 μM, ----- 7 μM, ... 10 μM, —.—.— 13 μM. DNA phosphate:(3) ratios: ∞:1, 100:1, 50:1, 33:1, 25:1, 18:1, 14:1.

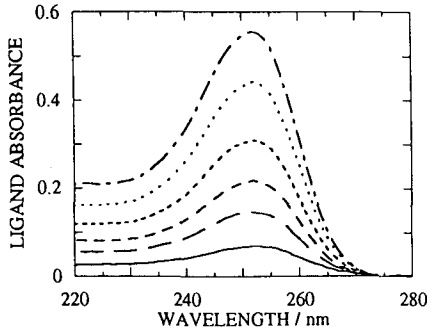

Fig. 3 Ligand absorbance determined from Fig. 2 spectra by subtracting 0 μM (3) spectrum from others. (3) concentrations: —— 2 μM, — — — 4 μM, – – – 5 μM, ----- 7 μM, ... 10 μM, —.—.— 13 μM. DNA phosphate:(3) ratios: 100:1, 50:1, 33:1, 25:1,18:1, 14:1.

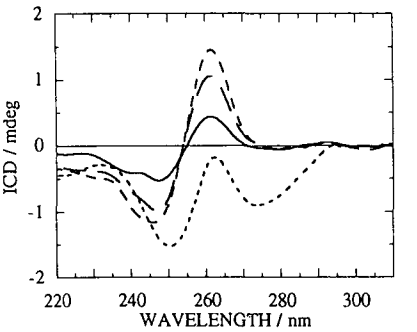

Fig. 4 Induced CD spectrum of (3) in 130μM calf thymus DNA, 5 mM NaCl, 1 mm pathlength. (3) concentrations: —— 7 μM, — — — 16 μM, – – – 24 μM, ----- 53 μM. DNA phosphate:(3) ratios: 19:1, 8:1, 5:1, 2.5:1.

Given the increasing interest in DNA curvature and bending, and in the influence of polyamines on this process, this transition may be of importance. It must be a DNA structural change, as the experiment only probes DNA base stacking. The melting transition occurs at 87°C for (**2**)-ct-DNA, and at 91°C for (**3**)-ct-DNA and corresponds to the helix to coil transition. The stability afforded by the spermine conjugate (**3**) is thus greater than that of spermine (**2**), despite the lower charge of the former. As (**1**)-ct-DNA has a melting temperature of 83°C, the intercalated moiety is approximately equivalent to two units of positive charge.

We have previously found [13] the most stable spectroscopically detectable binding mode of (**3**) with GC occupies ~3.5 base pairs and has an intercalated anthracene moiety. This mode dominates the spectra for GC until mixing ratios of 10:1 DNA phosphate-ligand are reached. At higher ligand concentrations, an additional GC complex with a groove-bound anthracene moiety is observed. For polyamine conjugate (**3**) with AT, preliminary experiments show constantly changing average binding behaviour as a function of ligand concentration. At extremely low ligand concentrations, only intercalative binding may be present, however, for AT, intercalative and non-intercalative binding modes seem to be energetically comparable.

To gain further insight into the molecular details of the specific binding geometries of (**3**), we have performed some simple molecular dynamics simulations on conjugate (**3**) with rigid AT and GC 18-mers. Such a computational approach offers a potential methodology for studying polyamine-DNA interactions, particularly if they are restrained by direct and indirect comparisons with experimental data. Two 400 ps simulations were performed for each sequence using a Silicon Graphics Indigo Workstation. The first of these used canonical B-DNA and the second a DNA duplex with a potential intercalation site. Literature evidence [14, 15] exists for both major- and minor-groove binding sites for spermine (**2**). In our simulations, we therefore initially located conjugate (**3**) orientated towards the DNA backbone, rather than towards either of the two grooves. During the initial period of dynamics, the ligand falls into the DNA helix and is then free to move across the surface of the DNA duplex. This method permits the ligand to locate favourable binding sites on the helix. In all simulations, the ligand was fully protonated and was assigned atomic point charges and force-field parameters derived from AM1 semi-empirical calculations. AMBER4.0 parameters were assigned to the DNA. The calculations excluded explicit water molecules using a distance dependent dielectric constant ($\varepsilon = 4r$) to modulate electrostatic interactions.

In the (**3**)-AT plus intercalation site simulation, we observed intercalation of the anthracene moiety after only 20 ps. The intercalated complex was maintained over the remainder of the simulation. The long axis of the anthracene remained essentially parallel with those of the base pairs of the intercalation site (Fig. 9). In the (**3**)-canonical AT simulation, we observed an initial, unstable major groove-backbone complexation in which no specific orientation was adopted. At 140 ps, the ligand moved to the minor groove, adopting a location in which the polyamine moiety lay, in an essentially all *trans* conformation, along the bottom of the groove, with the anthracene moving freely in and out of the groove. This minor-groove location was energetically better than major groove-backbone binding. However, the intercalated complex is only marginally less favourable than the non-intercalated minor-groove complex. We propose that these latter two complexes are equally probable, as it can reasonably be expected that inclusion of explicit water would increase the relative stability of the intercalated complex.

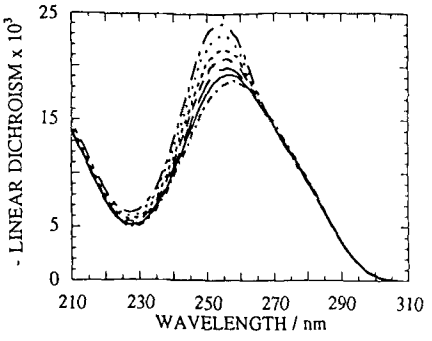

Fig. 5 -LD spectra of (3) in 180 μM calf thymus DNA, 5 mM NaCl, 1 mm pathlength. Concentrations and ratios as for Fig. 2.

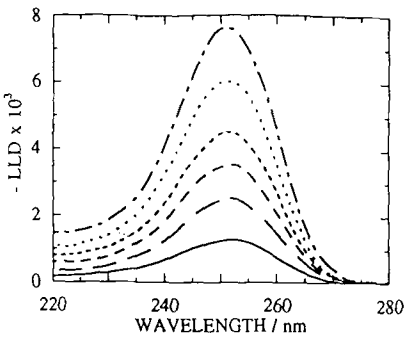

Fig. 6 -LLD spectra of (3) in 180 μM calf thymus DNA, 5 mM NaCl, 1 mm pathlength, determined as described in text. Concentrations and ratios as for Fig. 3.

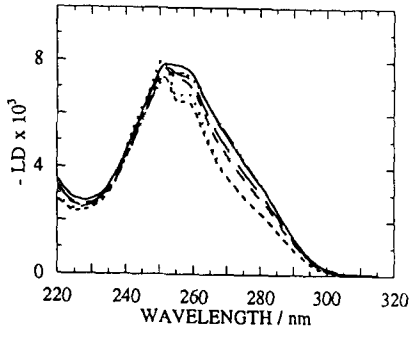

Fig. 7 -LD spectra of (3) in 130 μM calf thymus DNA, 5 mM NaCl, 1 mm pathlength. (3) concentrations: —·—·— 0 μM, —— 7 μM, — — — 16 μM, - - - 24 μM, ----- 53 μM. DNA phosphate:(3) ratios: ∞:1, 19:1, 8:1, 5:1, 2.5:1.

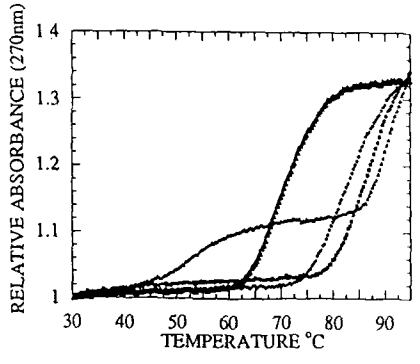

Fig. 8 Absorbance at 270 nm as a function of temperature of 200 μM calf thymus DNA in the presence of 5 mM NaCl (circles), 5 mM NaCl and 20 μM (1) (diamonds), 5 mM NaCl and 20 μM (2) (squares), 5 mM NaCl and 20 μM (3) (triangles). Data normalised to 1 at 30°C.

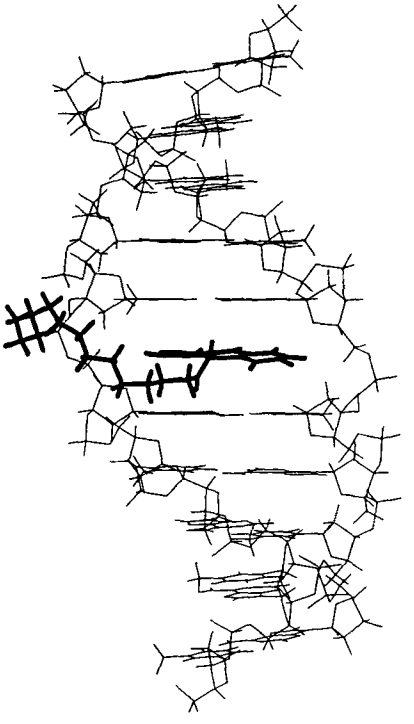

Fig. 9 Structure taken from the (3)/AT simulation showing (in bold) an intercalated anthracene moiety.

In the (**3**)-GC plus intercalation site simulation, we did not observe formation of an intercalated complex, although conformations close to intercalation were generated. However, as the ligand occupied a major groove or major groove-backbone location throughout the simulation, we conclude that the intercalation of (**3**) with GC occurs from the major groove and there is unlikely to be a minor-groove complex, either intercalated or non-intercalated.

The experimental data we have reported show that the most stable binding mode of spermine conjugate (**3**) has an intercalated anthracene moiety. In a second binding mode, the anthracene lies in a groove. For ct-DNA and GC, we believe that intercalated binding is favoured, but for AT, intercalative and non-intercalative binding modes are competitive. In accord with this, the computational results correspond to a single location for (**3**) with GC, but, with AT, to two equally probable locations, intercalative and minor-groove bound. This combined approach of experiment and theoretical calculation, each providing insight into results obtained from the other, is a potentially powerful method for elucidating the nature of polyamine-DNA interactions.

Acknowledgements: ST is supported by MRC G9219146N. ISB is the recipient of a Nuffield Foundation Science Lecturer's award (SCI/180/91/15/G). AR has a Glasstone Research Fellowship. ISH has support from the James H Zumberge Faculty Research and Innovation Fund, from an AACP New Investigators Grant, and from NCI (CA64299-01). Parts of this work were submitted by GA (University of Bath) and HCL (University of Oxford) as Part II Projects.

References

[1] Pegg, A. E.; Wechter, R.; Pakala, R.; Bergeron, R. J. *J. Biol. Chem.* **1989**, *264*, 11744-11749.

[2] Albanese, L.; Bergeron, R. J.; Pegg, A. E. *Biochem. J.* **1993**, *291*, 131-137.

[3] Basu, H. S.; Pellarin, M.; Feuerstein, B. G.; Deen, D. F.; Marton, L. J. *Int. J. Cancer* **1991**, *48*, 873-878.

[4] Basu, H. S.; Pellarin, M.; Feuerstein, B. G.; Deen, D. F.; Bergeron, R. J.; Marton, L. J. *Cancer Res.* **1990**, *50*, 3137-3140.

[5] Koza, R. A.; Herbst, E. J. *Biochem. J.* **1992**, *281*, 87-93.

[6] Basu, H. S.; Sturkenboom, M. C. J. M.; Delcros, J.-G.; Csokan, P. P.; Szollosi, J.; Feuerstein, B. G.; Marton, L. J. *Biochem. J.* **1992**, *282*, 723-727.

[7] Wemmer, D. E.; Srivenugopal, K. S.; Reid, B. R.; Morris, D. R. *J. Mol. Biol.* **1985**, *185*, 457-459.

[8] Marquet, R.; Houssier, C. *J. Biomol. Struct. Dyn.* **1988**, *6*, 235-246.

[9] Thomas, T. J.; Gunnia, U. B.; Thomas, T. *J. Biol. Chem.* **1991**, *266*, 6137-6141.

[10] Wakelin, L. P. G. *Med. Res. Rev.* **1986**, *6*, 275-340.

[11] Denny, W. A. *Anti-Cancer Drug Design* **1989**, *4*, 241-263.

[12] Baguley, B. C. *Anti-Cancer Drug Design* **1991**, *6*, 1-35.

[13] Rodger, A.; Blagbrough, I. S.; Adlam, G.; Carpenter, M. L. *Biopolymers* **1994**, *34*, in press.

[14] Schmid, N.; Behr, J.-P. *Biochemistry* **1991**, *30*, 4357-4361.

[15] Haworth, I. S.; Rodger, A.; Richards, W. G. *Proc. Roy. Soc. Lond.* B **1991**, *244*, 107-116.

(*Received in USA* 19 *July* 1994; *accepted* 14 *September* 1994)